Journal of Power Sources 208 (2012) 58–66

Contents lists available at SciVerse ScienceDirect

Journal of Power Sources

journal homepage: www.elsevier.com/locate/jpowsour

Effects of platinum on photo-assisted electrocatalytic activity of fringe-shaped highly ordered mesoporous titanium dioxide film

Yunxia Guo, Jianping He*, Shichao Wu, Tao Wang, Guoxian Li, Yuanyuan Hu, Hairong Xue, Xin Sun, Jing Tang, Mingzhu Liu

College of Material Science and Technology, Nanjing University of Aeronautics and Astronautics, Nanjing, Jiangsu 210016, PR China

ARTICLE INFO

Article history:
Received 26 September 2011
Received in revised form
16 December 2011
Accepted 1 January 2012
Available online 13 February 2012

Keywords:
Mesoporous
Titanium dioxide film
Photo-assisted electrocatalytic
Platinum modified

ABSTRACT

The platinum modified titanium dioxide film with highly ordered mesoporous framework is prepared by spin-coating method and applicated as the catalyst support material of direct methanol fuel cell, combining electro-photo catalysis innovately at different platinum (0–5 wt%) and anatase/rutile ratios. In this method, the well-ordered mesostructure with high-quality and large domain regularity are observed by field emission scanning electron microscope; meanwhile, platinum nanoparticles are homogeneous dispersed in the mesoporous framework of titanium dioxide films. As shown by the amperometric photocurrent–time curves and cyclic voltammetry, the overall photocurrent of 3 wt% platinum modified titanium dioxide film with UV irradiation is significantly 1.5 times higher than that of bare titanium dioxide film. This is further authenticated by the band gap data calculated and explained by electrochemical impedance spectroscopy measure results, which suggests that the superiority of platinum modified titanium dioxide film is attributed to the bicrystalline (anatase/rutile) framework, high crystallinity, mesoporous structure of films and the separation of photoinduced electron hole pairs.

1. Introduction

Nowadays, titania materials have attracted much attention owing to their unique optical–electronic properties, and potential applications in photocatalysis, chemical sensing [1,2], energy conversion and even water purification [3,4]. However, TiO_2 materials inevitably encounter a serious limit in following two aspects. To begin with, the disadvantages of titania is selective activity in the UV region (band gap 3.2 eV), which is only about 3–5% of the solar spectrum reaching the Earth's surface [5]. In the second place, TiO_2 materials generated photoinduced electrons and holes under illumination, which usually recombinated in a short time, resulting in poor optical performance.

As the addition of a noble metal to a semiconductor could effectively promote the electron–hole separation [6], better photocatalytic performance can be gained for direct methanol fuel cell (DMFC). In this case, metal nanoparticles are dispersed on the semiconductor surfaces, good catalytic activity can be obtained due to a so-called "support effect" or "synergistic effect" [7]. To the best of our knowledge, the coupling with noble metals has also been demonstrated to increase the photocatalytic activity by significantly prohibiting the fast recombination of photogenerated charge carriers. Nevertheless, the common carbon supported Pt or Pd nanoparticles catalyst suffers from some disadvantages such as poor loading, weak dispersion [8,9], and easy exfoliation of metal nanocatalyst [10,11] on supporting materials, which usually block the commercial application of DMFCs [12,13]. Therefore, many efforts have been devoted to improve the catalyst dispersion and support design. According to the literature, noble metals, e.g. (Pt [5], Ag, Au [6]), are effective dopants for visible light activation 1 by photoexciting surface plasmons in the metal atom. Wherein, the metal clusters act as sinks for the photogenerated conduction band electrons and reduce charge recombination. The presence of a metal at the surface of TiO_2 results in the formation of a Schottky barrier at the metal–semiconductor interface, which facilitates the interfacial electron transfer and subsequently encourages charge carrier separation. For instance, Kimberly A. Gray's group [5] prepared platinum-doped titania nanotubes by a hydrothermal technique to produce visible light activated catalysts, suggested the potential for practical applications such as incorporating Pt-doped titania nanotubes with commercially available light sources for indoor air purification. Meanwhile, mesoporous nanocrystalline TiO_2 have various fascinating properties such as large surface areas, controllable pore sizes, high adsorption capacity and large pore volumes as compared with the bulk or microsized counterparts, driving them used for a wide variety of potential applications in fields of adsorption, purification, catalysis, and energy storage [8].

In our view, what the most attractive thing is its methanol photocatalysis on pure or modified TiO_2. Reasons explained for this matter is that methanol is a common substrate molecule for

* Corresponding author. Tel.: +86 25 52112900; fax: +86 25 52112626.
E-mail address: jianph@nuaa.edu.cn (J. He).

0378-7753/$ – see front matter © 2012 Elsevier B.V. All rights reserved.
doi:10.1016/j.jpowsour.2012.01.006

photocatalytic performance evaluation [14,15] and can also be used as a sacrificial reagent [16,17] for photocatalytic hydrogen production [8,18]. To solve the problem, design of TiO_2 with well-defined mesoporous structure is a promising way to achieve high photocatalytic activity, since the ordered mesopore channels facilitate fast intraparticle molecular transfer [12,19], while the large surface area may enhance the light harvesting and the adsorption for reactant molecules [20,21]. Obviously, high crystallization degree of photocatalysts is favorable for rapid transfer of photocharges from bulk to surface, which could inhibit the recombination between photoelectrons and holes, leading to enhanced quantum efficiency. Besides, a proper spatial arrangement can further assist the electron/energy transfer within the mesoporous framework [18]. Based on those advantages of high crystallinity and mesostructural regularity of TiO_2 framework have received steady growing interest. Such materials can be readily formed by coassembly of inorganic oligomers with structure-directing agents using evaporation. He' group [3] prepare highly ordered mesoporous TiO_2 films with stripe-shaped mesochannels running parallel to substrates which are retained at 400 °C by the solvent-induced self-assembly (EISA)-derived method and exhibiting great potential in developing new generation DMFCs.

In this contribution, we report highly ordered hexagonal P6m mesoporous Pt/TiO_2 film at different Pt content (0–5 wt%) and anatase/rutile ratios as the novel photo-assisted catalyst of DMFC on the fluorine-doped SnO_2 transparent conductive (FTO) glass. In addition, the morphology and electronic properties of the photoelectrocatalysts were studied using electron paramagnetic resonance spectroscopic techniques. Most important of all, the mechanism of enhanced reactivity was probed by investigating the interactive effects caused by the conditions of synthesis and the Pt centers.

2. Experimental

2.1. Chemical materials

Poly(propylene oxide)-block-poly(ethylene oxide)-block-poly(propylene oxide) triblock copolymer Pluronic F127 (M_w = 12,600, $PEO_{106}PPO_{70}PEO_{106}$) was purchased from Sigma–Aldrich Corp., chloroplatinic acid (H_2PtCl_6) were purchased from Nanjing Ningshi Chemical Corp., $TiCl_4$ was purchased from Shanghai Meixing Chemical Corp., phenol, formalin solution (37 wt%), KOH, HCl, and ethanol were purchased from Shanghai Chemical Corp. All chemicals were used as received without any further purification. Deionized water was used in all experiments.

2.2. Preparation of mesoporous titanium dioxide films with platinum nanoparticles

For the synthesis of mesoporous Pt/TiO_2 composite film, triblock polymer F127 (M_w = 12,600, $PEO_{106}PPO_{70}PEO_{106}$) was used as a template, which is based on the previous report [22,23]. Typically, F127 was completely dissolved in ethanol, and then 1.12 ml of $TiCl_4$ and different amount of hydro-alcoholic solutions of chloroplatinic acid (H_2PtCl_6) were added with vigorous stirring at 40 °C for 30 min, the corresponding amount of distilled water was added to get a transparent sol solution.

The Pt/TiO_2 films were deposited by spin-coating at set rates onto the FTO substrate. Prior to coating, the FTO substrates were cut into (2 cm × 2 cm) specimens. The specimens were decreased using acetone; then washed in ethanol and distilled water, and finally dried in warm air. The as prepared solution was then spun onto the FTO substrate at 1500 rpm for 60 s using a SPINCOATER KW-4A. This procedure was repeated five times giving reproducible crack free thin films with strong adhesion between the Pt/TiO_2 and FTO surfaces.

The as-deposited samples were placed for 2 days to with relative humidity at 60% then thermo polymerized in an oven at 60 °C, 100 °C, 130 °C for 1d. Finally, highly ordered mesoporous transparent mesoporous Pt/TiO_2 films with narrow nanoscale pore size distribution and high ratio of surface area and pore volume can be obtained after removing the organic template by calcinations at 400 °C under air atmosphere. The resulting ordered mesoporous Pt/TiO_2 composite film is denoted as Pt/TiO_{2-x}, where x represented the mass percent of platinum in the films.

2.3. Film characterization

The powder X-ray diffraction (XRD) patterns were obtained using a Bruker D8 Advance diffract meter using a Cu Ka source (λ = 0.154056 nm) at 40 kV and 40 mA. Steady-state absorption measurements were performed at room temperature in a Varian Cary 50 UV–vis spectrophotometer. The field emission scanning electron microscopy (FE-SEM/EDXS) images were recorded on a Hitachi S-4800 microscope with an accelerating voltage of 15 kV, to observe the surface and cross-section image of the films. The films for FE-SEM measurements were applied on the Si substrate.

2.4. Photoelectrochemical measurement

For electrochemical studies, a conventional three-electrode single glass cell was employed. Pt wire and saturated Ag/AgCl electrodes were used as counter and reference electrodes, respectively. The working electrode was prepared by taking a homemade encapsulated on FTO with insulating tape, obligating an area of 1 cm^2. The electrochemical behavior of the Pt/TiO_2 electrodes was characterized by using the cyclic voltammetry technique in 0.5 M of KOH and 1.0 M of methanol aqueous solution at a scan rate of 20 mV s^{-1} in the range of −0.6 to 0.5 V(vs. SCE) until a stable state was reached. An integrated 8 W Xe lamp was employed as a UV excitation source (the wavelength range of 250–380 nm). Electrochemical impedance spectroscopy (EIS) measurements using Solartron 1260 frequency response analyzer coupled to Solartron 1287 potentiostat were obtained at frequencies between 100 kHz and 0.01 Hz. The amplitude of the sinusoidal potential signal was 5 mV. All photoelectrochemical measurements were performed on a CHI 660C.

3. Results and discussion

3.1. Platinum modified film charaterization

Mesoporous Pt/TiO_2 films have been synthesized through a simple EISA method followed by spin coating in the presence of the F127 triblock copolymer as the structure directing agent. It has been confirmed that complexation of metal precursor with the functional segment of the block copolymer is essential to accomplish distribution and phase specific dispersion of smaller particle size [24]. The mesostructural ordering and crystalline phase of Pt/TiO_2 films were characterized by XRD measurements (Fig. 1). The as-made sample shows a well-resolved peak, which can be indexed to the (10) Bragg reflections confirming an ordered 2D-hexagonal mesostructure of the P6mm space group [3,20]. The observed high intensity and the sharpness of the peak prove that a long-range order exists in the TiO_2 films. As can be seen from Fig. 3, the diffraction peak is retained with the platinum addition less than 3 wt%, indicating that the structural regularity is maintained. However, with the increasing of platinum addition, diffraction peak intensity decreased suggesting the ordering of mesoporous films

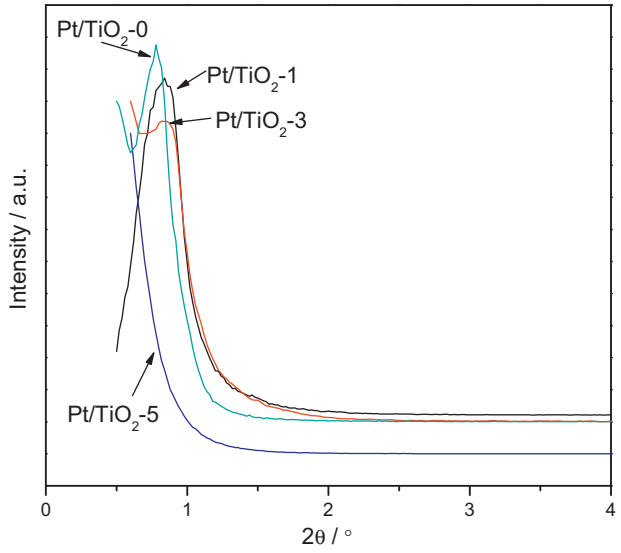

Fig. 1. Small-angle XRD patterns of continuous mesoporous film at different platinum content.

declined. When the amount of platinum at 5 wt%, the films diffraction patterns of small-angle XRD diffraction peak are not presence indicated that the ordered structure of mesoporous thin films were destroyed. The issue will be further explored with the assistance of WAXRD and FESEM analysis hereafter.

Fig. 2 shows the wide angle XRD patterns of the mesoporous Pt/TiO_2 films at different Pt contents. Clearly, the result of wide-angle XRD show that the pure TiO_2 nanoarchitectures begin to show reflections from anatase phases with peaks characteristic of the (1 0 1), (1 0 3), (2 0 0) of the anatase and (1 1 0), (2 1 1), (2 1 3) of the rutile lattice planes, suggesting that TiO_2 phase can nucleate and transform into nanocrystals at 400 °C. There are no indications for either rutile or brookite phases. However, with increasing Pt content, the peaks assigned to the anatase phase decrease and slightly rutile phase is formed and the signals at 40.5 and 46.2 correspond to the (1 1 1) and (2 0 0) planes of a face centered cubic Pt crystal structure, respectively. The quantitative phase composition and crystallite diameter of Pt/TiO_2 films at different Pt content and as evident from the Rietveld analysis of the XRD data are given in Table 1. Anatase and rutile mixtures are formed by the addition of Pt nanoparticles even at small concentration. These results indicate that there is a phase transformation from anatase to rutile

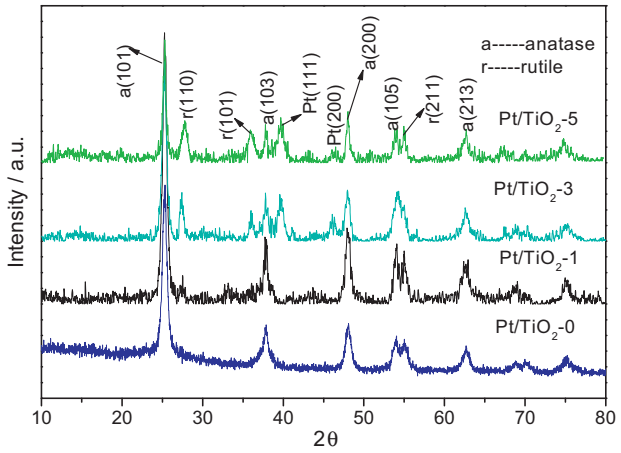

Fig. 2. High-angle XRD patterns of continuous mesoporous film at different platinum content.

Table 1
Percent of anatase/rutile of TiO_2, content and size of platinum particle calculated from XRD patterns.

Sample	Anatase (%)	Rutile (%)	Pt (%)	Size of Pt
Pt/TiO_2-0	99.14	0.825	0	–
Pt/TiO_2-1	93.295	6.520	0.185	15.15 nm
Pt/TiO_2-3	86.34	13.33	0.36	17.26 nm
Pt/TiO_2-5	83.41	16.17	0.42	18.68 nm

nanoparticles with Pt addition (Table 1). In particular, where this pure TiO_2 was present, no crystalline phase involving Pt can be observed, suggesting that either the Pt is highly dispersed in the TiO_2 network or that the Pt content is below the detection limit. On the other hand, at, 1, 3 and 5 wt% Pt/TiO_2, XRD patterns exhibit diffractions at around $2q = 39.8°$ and 46.3°, which can be indexed as (1 1 1) and (2 0 0) reflections of the crystalline Pt (JCPDF 01-1194) possessing a face-centered cubic structure with an Fm3m space group [25]. From what have been obtained in XRD data, the ratio of titanium dioxide crystal form of thin films and the size of platinum particles seemly have essential effect on mesoporous Pt/TiO_2 ordering. With the increased amount of Pt doping, the conversion of anatase to rutile easier. While beyond a certain weight percentage (3%), excessive platinum makes more conversion from the anatase to rutile phase, this over-conversion [20] process will destroy the mesoporous structure of thin films and reduce the ordering of the film (Fig. 3).

A more detailed structural characterization was revealed by FE-SEM imaging, as shown in Fig. 3a. In terms of test in our study, all samples were prepared by scraping off the films and dispersed in ethanol. As far as can be seen from SEM images of the calcined pure TiO_2 film, result indicates the well-ordered hexagonal arrays of mesopores with 2D channels with high quality and large-domain regularity of the TiO_2 film. It can be clearly seen that the mesoporous channels are straight and regularly array parallel to each other in the [1 1 0] direction for the TiO_2 film. Images (Fig. 3b) of mesoporous 1 wt% Pt/TiO_2 films calcined at 400 °C show that the doped film remains ordering mesoporous framework, maybe exist few platinum particles, but from the SEM images, we do not observe obvious platinum particle owe to spot of platinum addition. Fig. 3c (3 wt% Pt) demonstrates that platinum nanoparticles with an average diameter of about 20 nm particles are well dispersed and the film not agglomerated and destroyed [26]. This is corresponding to the result of XRD. And the elemental mapping (Fig. 4) aimed at platinum element on the surface of mesoporous Pt/TiO_2 (3 wt% Pt) suggested that platinum particles [27,28] are well dispersed on the surface of film [29,22].

3.2. Electrochemical photovoltaic characterization

The photoelectrochemical characteristics of methanol photoelectrochemical catalysis on and Pt/TiO_2 films were measured in 1.0 M CH_3OH + 0.5 M KOH aqueous solution. Fig. 5 shows the photocurrent response of the mesoporous TiO_2 film electrode and Pt/TiO_2 film electrode at different platinum content with and without UV illumination. Although the photocurrent of the bare mesoporous TiO_2 film electrode is only 10^{-7} A without UV illumination due to its low conductivity, whereas the photocurrent with UV illumination reaches as high as 0.6 mA cm^{-2}, 1000 times of the former. After Pt was doped on the mesoporous TiO_2 film, its conductivity improved, resulting in a significantly increased photocurrent of the Pt/TiO_2 film electrode whether with or without UV illumination. With the increasing of platinum, the photocurrent of Pt/TiO_2 films electrode obviously improved up to 0.80 mA cm^{-2}.However, when the amount of platinum at 5 wt%, the photocurrent of film electrode is not further increased, contrarily, the current decreased

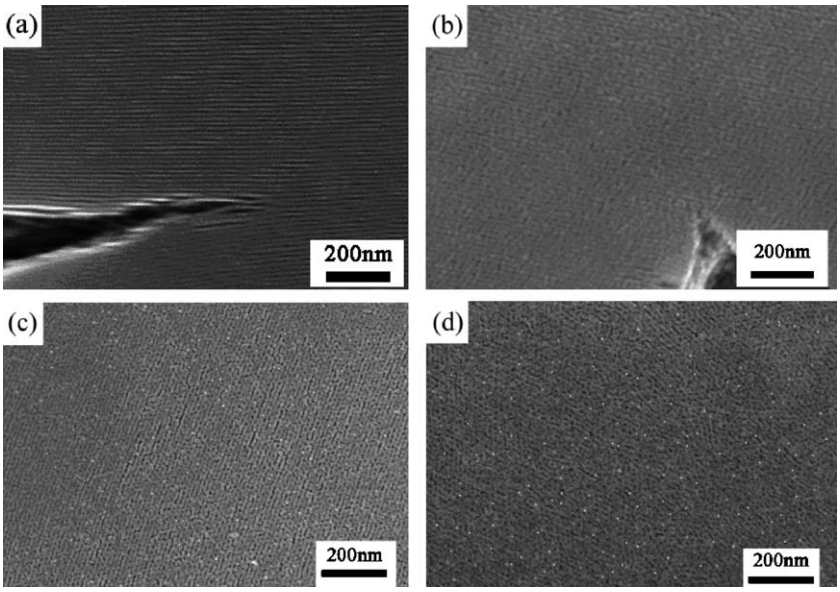

Fig. 3. FESEM images of different platinum content mesoporous Pt/TiO_2 films calcined at 400 °C for 4 h (a: 0 wt%, b: 1 wt%, c: 3 wt%, and d: 5 wt%).

to 0.5 mA cm^{-2}, even less than that of bare TiO_2 film. This mechanism is further discussed in latter CV measures.

The characteristics of methanol catalytic performance of the films were measured by cyclic voltammetry in 1.0 M CH_3OH + 0.5 M KOH aqueous solution. As TiO_2 is a wide band semiconductor [3], little current response (10^{-6} to 10^{-7} A) is observed for the bare TiO_2 film electrode in the dark (Fig. 6a), whereas an obvious photocurrent increase appears when the electrode is exposed to the UV illumination (Fig. 6b). From this figure the photocurrent of 1 wt% Pt was found to slightly increase than that of pure TiO_2 film electrode, but no obvious redox peaks are observed, indicating the bare TiO_2 film electrode has little catalytic performance for methanol oxidation with and without UV illumination. That is because that not enough platinum is exposed on the surface of the film. In the absence of UV illumination, with increasing Pt content at 3 and 5 wt% and the oxidation peak current then enhanced to 5.5×10^{-6} A and 7.8×10^{-6} A, respectively. Whereas, when the electrode is exposed to the UV illumination, a great oxidation peak current increase is observed as high as 12.3×10^{-4} A and 7.5×10^{-4} A, approximately 100 times of that without UV illumination, which agree to the *I–t* curves. This is also corresponding to the result of FE-SEM; platinum particles exposed on the surface of the film catalyzed the oxidation of methanol molecules. By introducing platinum into TiO_2 films, the current of Pt/TiO_2 films electrode increases sharply in the entire potential region and two methanol oxide peaks appear with and without UV illumination, revealing the photoelectrochemical oxidation of methanol. Fig. 6c displays the stability of electrical catalysis performance. In 100 cycles, the oxidation peak current increased at the first 20 cycles corresponding to the activation of the electrode. After 60 cycles,

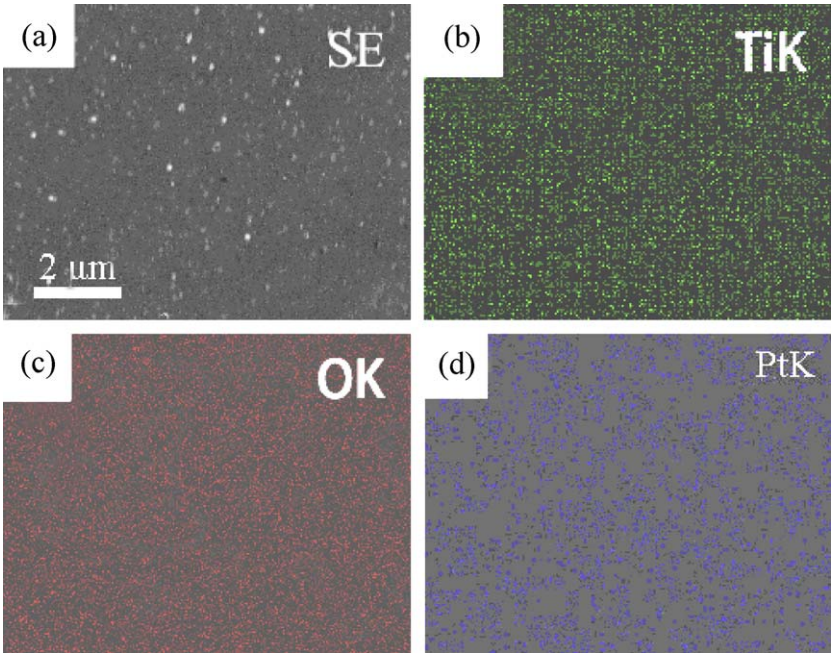

Fig. 4. Elemental mapping images of films at 3 wt% Pt doped film.

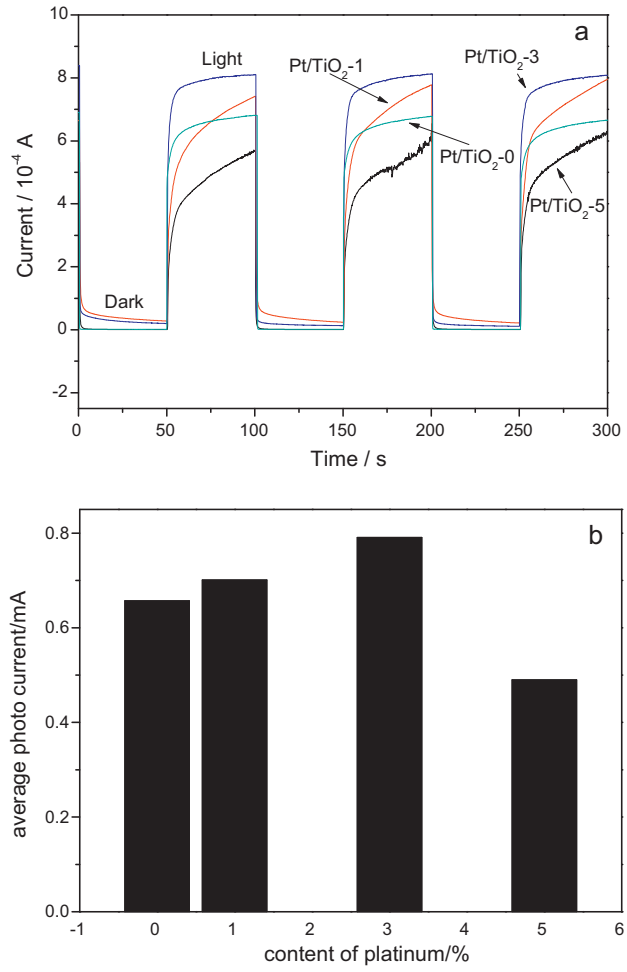

Fig. 5. a: *I–t* curves and b: average photo current with UV illumination of films electrode at different platinum content.

the current slightly decreased to 12.28 mA cm^{-2}, 99% of the stable current 12.34 mA cm^{-2}, remained the excellent resistance toxic performance.

In order to further search the oxygen reduction in alkaline solution, the tafel plot (Fig. 7) was measured in 1.0 M CH_3OH + 0.5 M KOH aqueous solution, calculated kinetic parameters is in Table 2. With ultraviolet radiation, the exchange current density is several mA cm^{-2}, 1000 times of that of without light (uA cm^{-2}), correspondingly, onset potential is more positive by 70 mV than that of without ultraviolet at 3%Pt content film electrode in alkaline solution. Furthermore, with the increasing of platinum content, the kinetic parameters in Table 2 has the trend of higher exchange current density (I_0) and more positive onset potential. But beyond the 3%Pt content, the onset potential is more negative and the exchange current density (I_0) is lower, this is consistent with the CV curves, which explained that the reaction mechanism of oxygen reduction for the role of platinum nanoparticles.

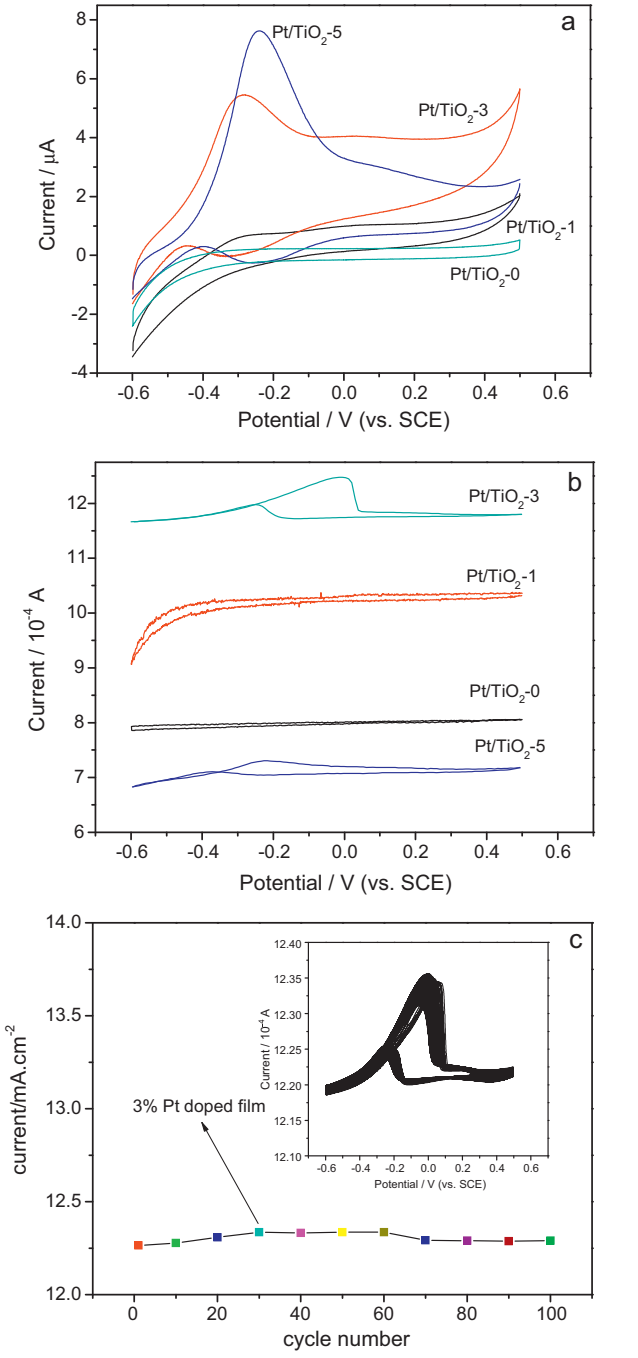

Fig. 6. CV curves of films at different platinum electrode content (a: without; b: with UV illumination; c: cycle performance of the 3%Pt content film, inset one is CV curves of 3%Pt content in 100 cycles).

Table 2
Comparison of kinetic parameters from tafel plot on different platinum content electrocatalysts with or without ultraviolet radiation.

Sample	I_0 (μA cm^{-2})	Onset potential (mV) (SCE)	I_0 (mA cm^{-2})	Onset potential (mV) (SCE)
	Light		Light	
0	2.04	−227	0.102	−100
1	3.12	−175	0.316	−50
3	5.24	−100	1.62	−29
5	2.29	−260	0.214	−34

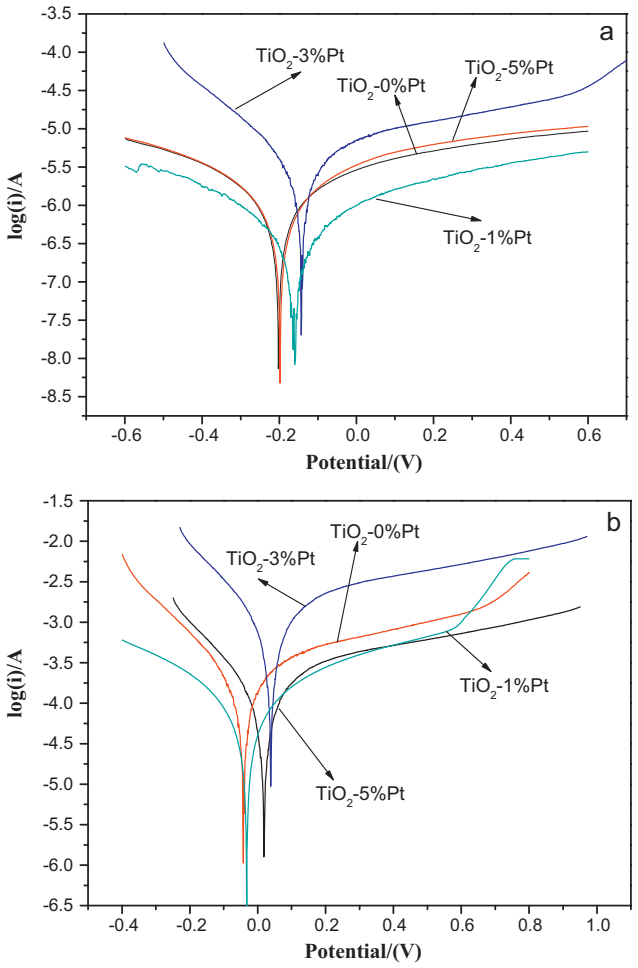

Fig. 7. Tafel plot of different platinum content films electrode (a: without and b: with UV illumination).

It is well-known that photoexcited electron–hole pairs (e–·····h+) form when TiO_2 is irradiated by UV light ($h\nu \geq 3.2$ eV) [6,30]. The electrons would transfer to the FTO glass substrate and generate a current response in the potential range from −0.6 to 0.5 V (vs. SCE). In turn, the holes can migrate to the surface of the TiO_2 and oxidize the electron donor species [30]. The surface holes can react with adsorbed water or hydroxyl to generate mobile •OH radicals, which have a high reactivity for oxidation of organic molecules [31,32]. In the case of methanol oxidation, the methanol molecules can react with the surface holes or •OH radicals to form various oxygen-containing intermediate species (•CH_2OH, CH_2O, CHO•, HCOOH, HCOO•, CO, etc.) and finally be mineralized to carbonate in alkaline media [13]. But, on the other hand, in competition with the charge transfer is the recombination of electrons and holes with the release of heat [15,27].

Considering the reaction dynamics during the entire photocatalytic process, the photocatalytic efficiency will be determined by the number of photogenerated charge carriers which can avoid the recombination reaction [33]. Incident photon to current conversion efficiency (IPCE) measurement is performed to further characterize the photoresponse of the three photoanodes. The IPCE was determined with no bias voltage by the following equation [34]:

$$\mathrm{IPCE} = \frac{1240\,(\mathrm{eV\,nm})}{\lambda\,(\mathrm{nm})} * \frac{\mathrm{Photocurrent\,(A)} * \mathrm{photodiode\ responsivity\,(V^{-1})}}{\mathrm{Photodiode\ photocurrent\,(A)}}$$

Table 3
Parameters evaluated by simulating the complex impedance plots from the EIS results and electrical conductivity of film electrode at different platinum content.

Sample	R_s (Ω)	R_{ct} (Ω)	CPE (μF)	L (S cm^{-1})	Band gap (eV)
Pt/TiO_2-0	153.5	75,454	0.6032	0.01625	3.43
Pt/TiO_2-1	142.7	74,500	0.8865	0.3466	3.39
Pt/TiO_2-3	84.76	60,900	0.9598	0.8667	3.01
Pt/TiO_2-5	19.23	100,500	0.6401	0.9456	3.26

The photocurrent was the total current under illumination minus the dark current, λ is the incident light wavelength. The electrolyte for was prepared shortly before photoelectrochemical measurements [35]. According the literature [13], photoexcited electron–hole pairs (e–·····h+) form when TiO_2 is irradiated by UV light ($h\nu \geq 3.2$ eV). The holes can migrate to the surface of the TiO_2 and oxidize methanol molecules to form various oxygen-containing intermediate species (•CH_2OH, CH_2O, CHO•, HCOOH, HCOO•, CO, etc.) and finally be mineralized to carbonate in alkaline media. The electrons would transfer to the FTO glass substrate and further moved the platinum nano-particles to oxidize methanol molecules. So the IPCE indirectly reflected the electrocatalytic activity of methanol oxidation.

Fig. 8a shows the IPCE results as a function of the irradiation wavelength for the mesoporous Pt/TiO_2 films at different Pt contents. As can be seen from Fig. 8, the IPCE increases with increasing Pt content up to 3 wt% Pt/TiO_2 with the maximum photonic efficiency being 13.5% under 330 nm wavelength, while in the presence of undoped mesoporous TiO_2 nanoparticles the photonic efficiency is 10.2%. Clearly, the mesoporous Pt/TiO_2 films are more photoactive than the bare TiO_2 film. Subsequently, the photonic efficiency gradually decreases to 10.26% with increasing Pt/Ti ratio reaching a value of 5 wt% Pt. Meanwhile, the peaks shift reward with the increase of platinum addition suggested narrower band gap, which is authenticated by the UV–vis absorption spectra and band gap data (Fig. 8b and c).

Electronic structures are usually associated with dielectric polarons and this was investigated via UV–vis diffusion reflectance spectroscopy for different platinum content. As shown in Fig. 8b, the curve of 3 wt% Pt modified film exhibits that a strong absorption due to the interband transition was observed at 450 nm, which gradually shift towards higher wavelength and become steeper with increased platinum addition, being at 370 nm for bare TiO_2 film. The band gap is estimated from the absorption edge wavelength of the interband transition according to the equation [36,37]. Fig. 8c exhibits a band-gap reduction from 3.43 to 3.01 eV with the platinum content from 0 to 3 wt%, lower than 3.2 eV of reported. The steepened adsorption edges and the red-shift gap might be characteristic of the surface defect dipoles and the size of platinum particles.

Impedance spectroscopy is efficient for characterizing the dielectric behavior of a material, especially nanomaterials of lower homogeneous structure [38], which also provide a powerful method for the study of charge transfer and recombined processes at the semiconductor/electrolyte interfaces [39]. For titanate, the existence of labile protons suggests that this material should have pronounced proton conductivity. A typical EIS plot obtained at room temperature in 1.0 M CH_3OH and 0.5 M KOH aqueous solution for as-prepared platinum modified TiO_2 films is shown in Fig. 9, and calculated data is Table 3. The corresponding equivalent circuit of films at different platinum content is shown in Fig. 10. First, the resistance R_S resulting from the solution, contacts, and the leads can be estimated from the real part of the EIS at very high frequencies [40]. The decreased trend of R_S for the increased platinum content films electrodes was observed, which indicated that the conductivity of the films. Thus, as seen from Table 3, the enhanced activities

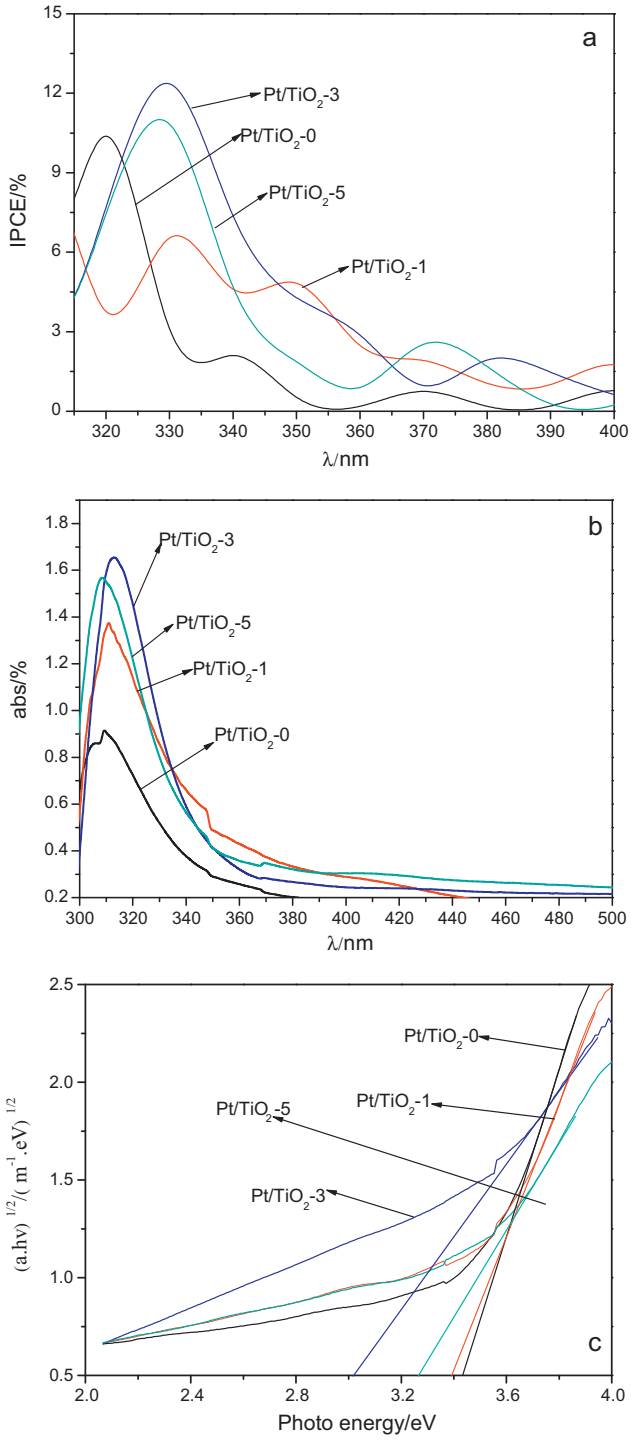

Fig. 8. a: IPCE results, b: UV–vis absorption spectra and c: band gap of film electrode at different platinum content.

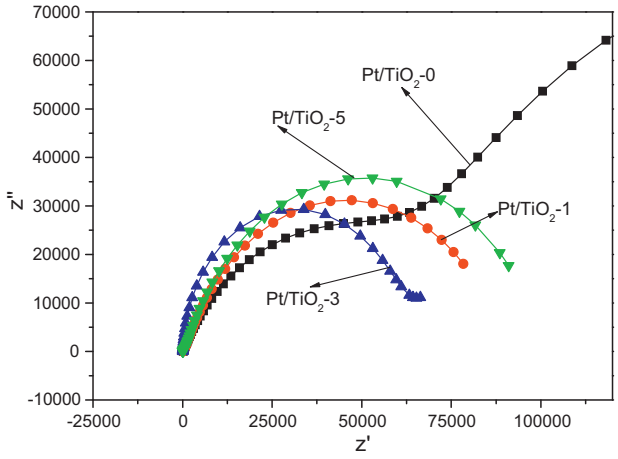

Fig. 9. Nynquist plots for films electrode at different platinum immersion in 1.0 M CH_3OH + 0.5 M KOH aqueous solution.

were attributed to the introducing of platinum. Second, as shown in the Nynquist plots, after doping of platinum, the visible EIS arc of the electrode becomes smaller at the same condition. According to the previous work [41], the smaller size of the semicircle arc diameter indicated a more effective separation of photogenerated electron–hole pair and/or a faster interfacial charge transfer to the electron donor/acceptor. In Fig. 8, a semicircle with near-zero intercept in the high frequency was observed, while exposed at surfaces, which likely lead to surface dangling bonds [42]. On the other hand, with the increase of platinum addition, the charge transfer resistance (R_{CT}) of 1 wt% and 3 wt% Pt are 74,554 Ω and 60,900 Ω, respectively, much less than the bare TiO_2 films (Table 3), indicating that more excellent proton transfer capability and effective separation of photogenerated electron–hole pair is achieved by the platinum addition, whereas, as the increase of platinum content, the platinum addition is up to 5%, the charge transfer resistance increased to 100,500 Ω, in good agreement with what the IPCE results (Fig. 8).That also explained the 3 wt% Pt film have the optimal photoelectrochemical characterization.

This difference can be attributed to several effects, such as a lower light scattering effect of the ordered mesopores, an accumulated local concentration of •OH [43], or a fast transport of the target molecule CH_3OH to the active sites due to the facile diffusion of the CH_3OH through the ordered porous network, which for the samples are hindered by the heterogeneities existing in the bulk sample difference in activity found for undoped mesoporous TiO_2 and doped ones thus suggests that the rate of electron transfer from mesoporous TiO_2 nanocrystals to adsorbed oxygen is increased when Pt is incorporated into mesoporous TiO_2. This will lead to better charge carrier separation and thus to an increase of the photocatalytic activity. In three-dimensional solid/surface state mesoporous framework, the excited TiO_2 nanoparticle can transfer the absorbed energy through the mesoporous hexagonal TiO_2 network to other ground-state TiO_2 [19]. Through the so-called antenna mechanism the resulting energetic coupling throughout a three-dimensional TiO_2 network will enable an energy and/or exciton transfer from the particle where the initial photon absorption took place to the particle where the electron transfer process finally occurs. Consequently, the probability of electron transfer to the Pt particle is increased by an increased CH_3OH diffusion through the pores of the nanostructures.

Moreover, we can find that too much anatase will retard the photodegradation process, indicating that the proper amount of rutile is of certain benefit (Fig. 11). Such a synergetic effect, also referred to as 'mixed phase effect', is supposed to efficiently prohibit the recombination of photogenerated electron–hole pairs by transferring the exited electrons from one phase to another [38]. Therefore,

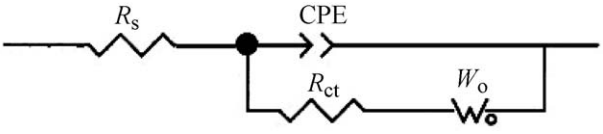

Fig. 10. Equivalent circuit of films electrode at different platinum content in 1.0 M CH_3OH + 0.5 M KOH aqueous solution.

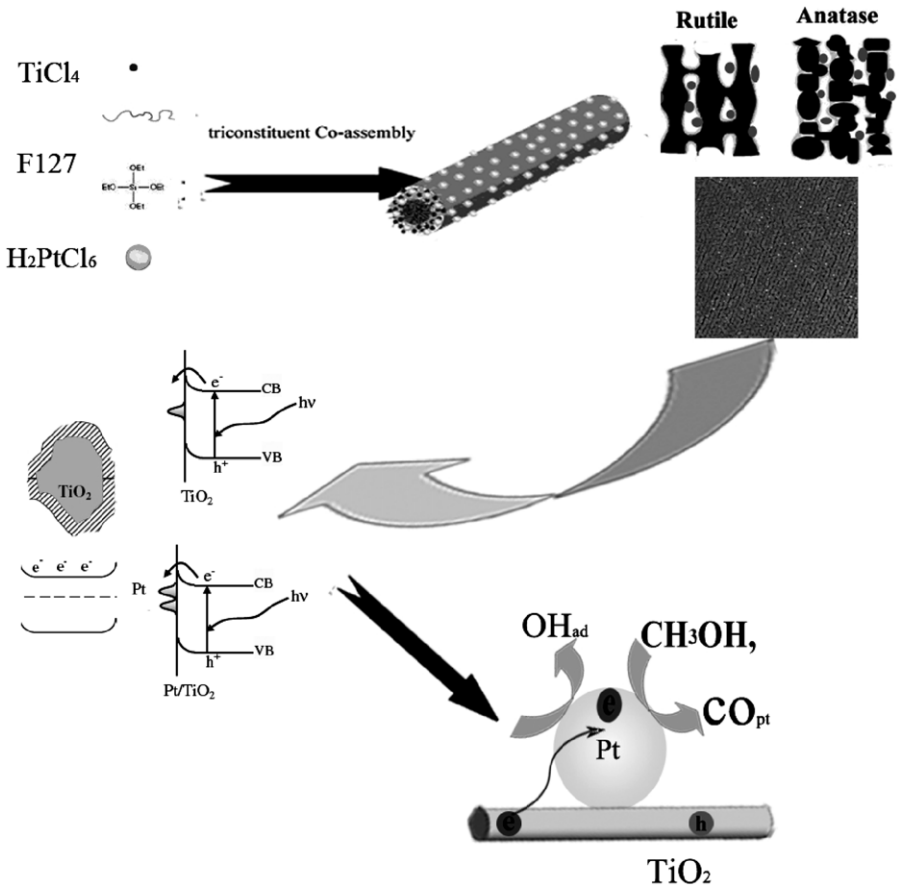

Fig. 11. Schematic illustration of preparation of the Pt/TiO_2 films.

both the regular open pore morphology and the biphase structure are playing crucial roles in determining the sample's photoactivity. Some report seem to demonstrate that rapid electron transfer, occurring from rutile conduction band to lower energy anatase lattice trapping sites in mixed-phase, leads to a more stable charge separation. The electron-transfer process causes the existence of catalytic hot spots at anatase/rutile interface [44].

Another explanation for the higher photocatalytic activity might be the size of the Pt particles. This has been attributed to a rate control by rather slow reduction of molecular oxygen by the trapped photoelectrons, whereby e−/h+ recombination is favored [15]. The purpose of loading TiO_2 with Pt is to generate at the interface between Pt and TiO_2 a Schottky barrier, which effectively captures the photogenerated electrons and reduces the rate of electron–hole recombination [32]. The interface being maximum at low Pt nanoparticles content and high dispersion, too large Pt particles (more than 3 wt%) could also act as recombination centers, detrimental to photocatalysis by hindering or avoiding the active photogenerated charge transfer to the reactant species at the surface. Therefore, the highest activity observed for the 3 wt% Pt/TiO_2 films can be ascribed to the most efficient charge separation through the mesopore charge transfer [45,46].

4. Conclusions

The fringe-shaped highly ordered mesoporous platinum modified titanium dioxide film at different platinum (0–5 wt%) and anatase/rutile ratios was prepared on the FTO. We find that the overall photocurrent of 3 wt% Pt/TiO_2 film with UV irradiation is significantly 1.5 times higher than that of bare TiO_2 film. In our case, the advantage of Pt/TiO_2 film is attributed to its bicrystalline framework, high crystallinity, mesoporous structure and the separation of photoinduced electron hole pairs. What is more, the regular open pore morphology and the biphase structure are playing crucial roles in promoting the diffusion of reactants and products, enhancing the photocatalytic activity by facilitating access to the reactive sites on the surface of photocatalyst.

Acknowledgement

This work is supported by the National Natural Science Foundation of China (Grant No. 50871053).

References

[1] S.Y. Huang, P. Ganesan, S. Park, J. Am. Chem. Soc. 131 (2009) 13898.
[2] A. Ismail, D.W. Bahnemann, L. Robben, V. Yarovyi, M. Wark, Chem. Mater. 22 (2010) 108.
[3] S.C. Wu, J.P. He, J.H.T.W. Zhou, Y.X. Guo, J.Q. Zhao, X.C. Ding, J. Mater. Chem. 21 (9) (2011) 2852–2854.
[4] W.Y. Dong, Y.J. Sun, C.W. Lee, W.M. Hua, X.C. Lu, Y.F. Shi, S.C. Zhang, J.M. Chen, D.Y. Zhao, J. Am. Chem. Soc. 129 (2007) 13894–13904.
[5] B.J. Kanna, V. yan, N.M. Dimitrijevic, J.S. Wu, K.A. Gray, J. Phys. Chem. C 114 (2010) 20917–20924.
[6] C.C. Jia, H.M. Yin, H.Y. Ma, R.Y. Wang, X.B. Ge, A.Q. Zhou, X.H. Xu, Y. Ding, J. Phys. Chem. C 113 (2009) 16138–16143.
[7] (a) M.S. Chen, D.W. Goodman, Science 306 (2004) 252;
(b) D.I. Enache, J.K. Edwards, P. Landon, B. Solsona-Espriu, A.F. Carley, A.A. Herzing, M. Watanabe, C.J. Kiely, D.W. Knight, G.J. Hutchings, Science 311 (2006) 362;
(c) J.A. Rodriguez, S. Ma, P. Liu, J. Hrbek, J. Evans, M. Perez, Science 318 (2007) 1757;
(d) M. Valden, X. Lai, D.W. Goodman, Science 281 (1998) 1647.
[8] M. Okumura, S. Tsubota, M. Iwamoto, M. Haruta, Chem. Lett. 10 (1998) 315.
[9] Z.D. Wei, L.L. Li, Y.H. Luo, C. Yan, C.X. Sun, G.Z. Yin, et al., J. Phys. Chem. B 110 (2006) 26055e61.

[10] E.S. Steigerwalt, G.A. Deluga, D.E. Cliffel, C.M. Lukehart, J. Phys. Chem. B 105 (2001) 8097e101.
[11] I. Bannat, K. Wessels, T. Oekermann, J. Rathousky, D. Bahnemann, M. Wark, Chem. Mater. 21 (8) (2009) 1645–1653.
[12] H.X. Li, Z.F. Bian, J. Zhu, Y.N. Huo, H. Li, Y.F. Lu, J. Am. Chem. Soc. 129 (15) (2007) 4538–4539.
[13] N. Venkatachalam, M. Palanichamy, B. Arabindoo, V. Murugesan, Catal. Commun. 8 (7) (2007) 1088–1093.
[14] C.Y. Wang, J. Rabani, D.W. Bahnemann, J.K. Dohrmann, J. Photochem. Photobiol. A 148 (2002) 169.
[15] T. Kawahara, Y. Konishi, H. Tada, N. Tohge, S. Ito, Langmuir 17 (2001) 7442.
[16] J. Marugan, D. Hufschmidt, M.J.Lopez-Munoz, V. Selzer, D. Bahnemann, Appl. Catal. B 62 (2006) 201.
[17] P.V. Kamat, J. Phys. Chem. C 111 (2007) 2834.
[18] H. Shibata, T. Ogura, T. Mukai, T. Ohkubo, H. Sakai, M. Abe, J. Am. Chem. Soc. 127 (2005) 16396.
[19] A.A. Ismaila, D.W. Bahnemannb, Green Chem. 13 (2011) 428.
[20] J.C. Yu, G.S. Li, X.C. Wang, X.L. Hu, C.W. Leung, Z.D. Zhang, Chem. Commun. (2006) 2717.
[21] (a) A.A. Ismail, D.W. Bahnemann, Chem. Sust. Chem. 3 (2010) 1057–1062;
(b) A.A. Ismail, T.A. Kandiel, D.W. Bahnemann, J. Photochem. Photobiol. A 216 (2010) 183–193.
[22] T. Wang, J.P. He, D. Sun, et al., Corros. Sci. 53 (2011) 1489.
[23] Y. Meng, D. Gu, D.Y. Zhao, Angew. Chem. Int. Ed. 44 (2005) 7053.
[24] N.R. Mayavan, Choudhury, N.K. Dutta, Adv. Mater. 1–6 (2008) 9999.
[25] Y.M. Liang, H.M. Zhang, Z.Q. Tian, X.B. Zhu, X.L. Wang, B.L. Yi, J. Phys. Chem. B 110 (2006) 7828.
[26] A. Tonscheidt, P.L. Ryder, N.I. Jaeger, G. Schulz-Ekloff, Surf. Sci. 281 (1993) 51–61.
[27] Y. Ting, Y.H. Deng, L. Wang, D.Y. Zhao, et al., Adv. Mater. 19 (2007) 2301–2306.
[28] S. Tominaka, C.W. Wu, T. Momma, K. Kurodab, T. Osaka, Chem. Commun. (2008) 2888–2890.
[29] A.L. Schmitt, J.M. Higgins, S. Jin, Nano Letters 8 (2008) 810–815.
[30] A.L. Linsebigler, G. Lu, J.T. Yates Jr., Chem. Rev. 95 (1995) 735.
[31] G.P. Wu, T. Chen, W.G. Su, G.H. Zhou, X. Zong, Z.B. Lei, C. Li, J. Int. Hydrogen Energy 33 (2008) 1243.
[32] A. Yamakata, T.A. Ishibashi, J.J. Onishi, Phys. Chem. B 107 (2003) 9820.
[33] M.R. Hoffmann, S.T. Martin, W. Choi, D.W. Bahnemann, Chem. Rev. 95 (1995) 69–96.
[34] L.P. Liu, J. Hensel, R.C. Fitzmorris, Y.D. Li, J.Z. Zhang, J. Phys. Chem. Lett. 1 (2010) 155–160.
[35] (a) D. Lawless, N. Serpone, D. Meisel, J. Phys. Chem. 95 (1991) 5166–5170;
(b) S. Tojo, T. Tachikawa, M. Fujitsuka, T. Majim, Chem. Phys. Lett. 384 (2004) 312–316.
[36] K.M. Reddy, S.V. Manorama, A.R. Reddy, Mater. Chem. Phys. 78 (2002) 239–245.
[37] A.S. Bnrnard, L.A. Curtiss, Nano Letters 5 (7) (2005) 1261–1266.
[38] W.B. Hu, L.P. Li, W.M. Tong, G.S. Li, T.J. Yan, J. Mater. Chem. 7 (2010) 900–906.
[39] X.F. Cheng, W.H. Leng, D.P. Liu, Y.M. Xu, J.Q. Zhang, C.N. Cao, J. Phys. Chem. C 112 (2008) 8725–8734.
[40] J. Bisquert, G. Garcia-Belmonte, F. Fabregat-Santiago, N.S. Ferriols, P. Bogdanoff, E.C. Pereira, J. Phys. Chem. B 104 (2000) 2287–2297.
[41] W.H. Leng, Z. Zhang, S.A. Cheng, J.Q. Zhang, C.N. Cao, Chin. Chem. Lett. 12 (2001) 1019.
[42] X.M. Song, J.M. Wu, M.Z. Tang, B. Qi, M. Yan, J. Phys. Chem. C 112 (49) (2008) 19484.
[43] D. Sukkim, S.-Y. Kwak, Environ. Sci. Technol. (2009).
[44] D.C. Hurum, A.G. Agrios, K.A. Gray, T. Rajh, M.C. Thurnauer, J. Phys. Chem. B 107 (2003) 4545.
[45] S. Yin, H. Hasegawa, D. Maeda, M. Ishitsuka, T. Sato, J. Photochem. Photobiol. A 163 (2004) 1.
[46] (a) N. Lakshminarasimhan, E. Bae, W. Choi, J. Phys. Chem. C 111 (2007) 15244;
(b) Y. Huang, W. Ho, S. Lee, L. Zhang, G. Li, J.C. Yu, Langmuir 24 (2008) 351.